Charles University
Faculty of Mathematics and Physics

HABILITATION THESIS

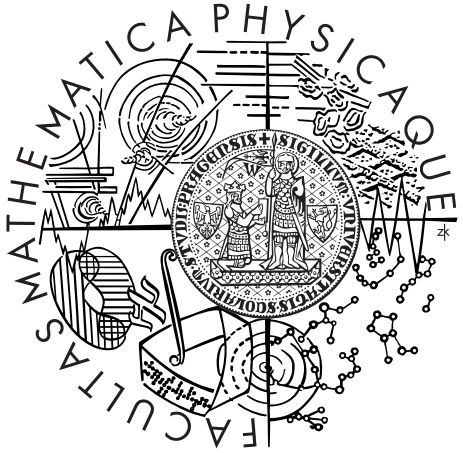

Cryogenic Fluid Dynamics and Quantum Turbulence

RNDr. David Schmoranzer, Ph.D.

Condensed Matter Physics

Prague 2019

Preface

This Thesis brings together the results of experimental investigations into cryogenic fluid dynamical problems such as quantum turbulence in superfluid helium or thermal convection in cryogenic fluids to which the author contributed during his work at the Faculty of Mathematics and Physics at Charles University, complemented by his work on the development of novel ultra-low temperature refrigeration techniques during his post-doctoral stay at the Institut Néel in Grenoble, France.

The Thesis takes the form of a commentary describing the main results obtained in each area, with focus on superfluidity and quantum turbulence. The details may be found in the author's original publications attached to the Thesis. For the reader's convenience, each paper is summarized in a short overview providing information about the principal results and cornerstone experimental techniques, as well as detailing the author's contribution.

The research presented in this Thesis has been supported primarily by the Czech Science Foundation, internal grants from Charles University, as well as by an ERC Starting Grant awarded to Dr. Andrew Fefferman at the Institut Néel in Grenoble.

Finally, I would like to take this opportunity to thank all my friends and colleagues without whom the presented work could never have been completed. My thanks belong to my present and former colleagues from the Prague Laboratory of Superfluidity: Ladik Skrbek, Miloš Rotter, Marco La Mantia, Martin Jackson, Simone Babuin, Daniel Duda and Emil Varga, as well as all the students working with us now. From the numerous collaborators abroad, I would like to thank specifically to Andrew Fefferman, Eddy Collin, Annina Luck, Sébastien Triquenaux, Philippe Roche and Henri Godfrin from the Institut Néel in Grenoble, to Viktor Tsepelin, Malcolm Poole, Rich Haley, Peter McClintock and George Pickett from Lancaster University, to Jaakko Hosio, Petri Heikkinen, Jere Mäkinen, Volodya Eltsov and Matti Krusius from Aalto University in Espoo, Finland, and to Grisha Sheshin from the B. Verkin Institute in Kharkiv, Ukraine. My most sincere thanks belong also to my close friends and family who have been very supportive of my work and showed a great deal of understanding for the day-to-day reality of experimental physics research.

Contents

1. Introduction

The general field of low temperature physics offers many interesting areas of research combining typical condensed matter topics such as microscopic mechanics of crystalline and amorphous solids, their magnetic properties, superconductivity or nanoscale phenomena at the quantum limit, with other themes connected perhaps more intimately to fluid dynamics, such as superfluidity or quantum turbulence. The latter class of topics represents the author's close specialization and the bulk of his contribution to the field, as reflected in this Thesis, but work on other low-temperature physics topics is included as well. For the purposes of clarity, these topics will be treated separately in the following Chapters and supported by original publications in the Appendix.

The dominant part of the Thesis is devoted to experimental investigations in the area of flow dynamics of superfluid helium and quantum turbulence, with focus on superfluid ^{4}He, detailed in Chapter 2. The same Chapter includes also experimental investigations of Andreev reflection on a rectilinear array of quantized vortices in the rare isotope of helium, specifically in the superfluid phase ^{3}He-B, performed during two visits to the Low Temperature Laboratory at Aalto University in Helsinki.

The normal liquid and vapour phases of ^{4}He are also readily used to explore another important topic in fluid dynamics – convective heat transfer. In collaboration with the Institute of Scientific Instrumentation in Brno, CZ, two-phase convection in liquid/gaseous helium was investigated, and the somewhat surprising observation of heat flux against the temperature gradient is explained in Chapter 3.

Finally, the development of a sub-millikelvin Continuous Nuclear Demagnetization Refrigerator (suitable for experimentation with the superfluid phases of ^{3}He as well as for ultra-low temperature condensed matter experiments) that was undertaken during the author's post-doctoral stay at the Institut Néel in Grenoble is detailed in Chapter 4.

2. Superfluidity and Quantum Turbulence

Superfluidity [1,2], i.e., fluid behaviour governed by quantum rather than classical physics, which may manifest as frictionless flow, emerges in several systems known to-date, most notably in superfluid phases of ^{3}He and ^{4}He, and in gaseous Bose-Einstein condensates – dilute clouds of laser-cooled atoms. While the properties of He II, the superfluid phase of ^{4}He are relatively well-known on the phenomenological level (Landau's two-fluid model), a full-fledged microscopic description is still missing. Superfluid phases of ^{3}He may be described by loose analogy with the BCS theory for superconductors [3]. However, the complexity of its order parameter guarantees very rich behaviour with many open questions. To this day, novel phases in confined geometries [4, 5] and new types of excitations [6] and topological defects [7] are being discovered in ^{3}He.

Quantum turbulence [8] is a peculiar type of turbulent flow that occurs in quantum fluids such as the superfluid phases of both helium isotopes. It differs from its classical counterpart in several important aspects, most notably the existence of quantized vortices, due to quantum-mechanical constraints of fluid circulation. For example in ^{4}He, the circulation quantum is given as $\kappa = h/m_4$, where h is the Planck constant and m_4 the mass of a ^{4}He atom [9]. Additionally, superfluids are typically described within the so called two-fluid model [10] as if consisting of two independent inter-penetrating components. One, the superfluid component, behaves as an inviscid Eulerian fluid with no entropy content, while the other, the normal component, has both entropy and viscosity. The relative ratio of the densities of these two components is determined by temperature and pressure, with the normal component dominating near the superfluid transition (at "high" temperatures). As the temperature is reduced, the density of the normal component rapidly decreases and at very low temperatures (for ^{4}He, of order 100 mK), only pure superfluid remains [1]. At any finite temperature, both components must be considered, and depending on the type of flow, turbulence may, in principle, develop independently in either of them.

Quantum turbulence may be investigated by many different techniques, ranging from traditional approaches such as stationary or vibrating mechanical objects [11] (see also Section 2.1), via specialized techniques available only in superfluids like second sound attenuation [12], which is typically used in ^{4}He above 1 K, or Andreev reflection of thermal excitations [13] in superfluid ^{3}He-B, to modern powerful approaches adapted from classical fluid dynamics, like Particle Imaging/Tracking Velocimetry [14, 15]. It is worth to mention that in the zero temperature limit (pure superfluid), any turbulent flow must be built up from individual quantized vortices of identical circulation, each satisfying the Kelvin theorem (vortices must end on container walls, free surfaces, or form closed loops). This makes quantum turbulence, at least in the zero temperature limit, a much simpler system to study than turbulence in classical viscous fluids [8], where vortices are constrained neither by a fixed value of circulation nor the Kelvin theorem which applies only to ideal fluids [16].

A significant part of the results presented below relate to the description of

two-component flows of superfluid ^{4}He, specifically to the scaling of drag forces acting on various oscillating systems in laminar regime and to the type of instability that triggers turbulence. The governing quantities describing the flow and controlling the instabilities are expressed, wherever possible, as suitably chosen dimensionless parameters (see below). However, for the description of pure superfluid, the fluid velocity U as such is often used [17], or for oscillatory flows, its dimensionless form may be obtained as $\hat{U} = U/\sqrt{\kappa\omega}$, where ω is the angular frequency of oscillation [18]. These results are presented in the first two Sections of this Chapter, while two additional Sections are devoted to the investigations of acoustic emission by oscillators immersed in superfluid ^{4}He undertaken by the Prague superfluidity group and to measurements of Andreev reflection of thermal excitations by a rectilinear array of quantized vortices in ^{3}He-B, performed during two visits of the author to the Low Temperature Laboratory at Aalto University in Helsinki.

2.1 Two-fluid Oscillatory Flows in Superfluid ^{4}He

Traditional probes of superfluid helium and quantum turbulence include vibrating objects, resonators of various shapes and sizes such as discs/spheres suspended on a torsion rod [19], vibrating superconducting wires [20,21], grids [22,23], vibrating microspheres [24,25], or piezoelectric tuning forks [26]. The resonators are used to measure the force-velocity response of the fluid and hence determine the moment of departure from the linear damping expected at low velocities, where the normal component flow is laminar and the superfluid component exhibits purely potential flow, therefore contributing zero drag as per d'Alembert's paradox [16]. Such a departure from linearity is then usually understood to signify an instability leading to the onset of turbulent flow [19–26].

The Prague group has been one of the first to successfully use quartz tuning forks to probe superfluid ^{4}He, which led, among other, to the description of the production of quantum turbulence [27,28], the detection of cavitation in both normal and superfluid helium [29–31], and to the observation of acoustic emission by the fork – a parasitic energy dissipation mechanism with profound implications for future sensor design and production [32,33]; the full articles are attached in Appendices A3 and A4.

In order to fully understand the turbulent transitions due to the normal or superfluid component, it is first necessary to provide a reliable and robust description of the linear drag forces. To achieve this goal, diverse types of oscillators have to be used in dedicated experiments. The long-standing effort of the Prague group to find a universal description of the drag forces culminated in the recent publication of Ref. [34] (attached in Appendix A1), where the relevant dimensionless parameter is identified and named after R. J. Donnelly (University of Oregon) who first proposed its use in his pioneering work on oscillatory flows of superfluid helium [19], but could not fully realize its importance due to the limited extent of experimental tools and data available at the time. The *Donnelly number* is defined as follows:

$$\mathrm{Dn} = \frac{U\rho_\mathrm{N}\delta_\mathrm{N}}{\eta}, \tag{2.1}$$

where U is the peak velocity (amplitude), ρ_{N} the density of the normal component, η the dynamic viscosity, and δ_{N} the viscous penetration depth of the normal component, $\delta_{\mathrm{N}} = \sqrt{2\eta/(\omega\rho_{\mathrm{N}})}$. Together with the flow geometry, Dn fully determines the observed laminar drag forces acting on bodies oscillating at sufficiently high frequencies, as determined by the condition that the normal component Stokes number $\beta_{\mathrm{N}} = D^2/(\pi\delta_{\mathrm{N}}^2) \gg 1$, with D the typical size of the object. This condition is satisfied for all the oscillators used in our work, and the laminar drag coefficient of the normal component $C_{\mathrm{D}}^{\mathrm{N}}$ is found for all the oscillators simply as:

$$C_{\mathrm{D}}^{\mathrm{N}} = \frac{\Phi}{\mathrm{Dn}}, \tag{2.2}$$

where the constant Φ is determined solely by the oscillator geometry and may be calculated exactly for many resonators; for details see Ref. [34] included in Appendix A1.

By determining, whether it is a critical value of the Donnelly number or rather a critical (dimensionless) velocity that controls the turbulent instability, this approach further allowed us to construct the scenarios of the transition in superfluid ^{4}He in flows past oscillating objects such as wires, discs or tuning forks. We have shown for the first time that either component (normal or superfluid) may trigger the transition to turbulence via independent mechanisms. We have also demonstrated that even in ^{4}He the superfluid component may be turbulent while the normal component exhibits laminar flow – a scenario previously considered only for superfluid phases of ^{3}He, due to the significantly higher viscosity of its normal component. The details are again given in Ref. [34], Appendix A1.

2.2 Turbulent Transition in Pure Superfluid ^{4}He

The question of how quantum turbulence develops in a system with no influence of the viscous normal component has been at the forefront of experimental and theoretical research ever since physicists had had access to millikelvin temperatures, which are sufficient for superfluid ^{4}He to enter such a regime [1]. Experimental observations (using vibrating wires or grids) were reported of not one, but rather two critical velocities, related to different regimes of quantum turbulence [22, 35–38]. The traditional interpretation stated that at the first critical velocity, vortex loops proliferated along the surface of the oscillator. There was, however, no clear consensus as to whether dissipative processes occurred at this stage, as part of the published works reported dissipationless flow [22, 38], while a change in dissipation was observed in other experiments [35–37]. At the second critical velocity, it was believed, a dense tangle of quantized vortices formed in the vicinity of the oscillating body (sustained by its kinetic energy), marking the onset of quantum turbulence as such [37, 38].

Using custom-made tuning forks, designed specifically to suppress parasitic effects such as acoustic losses and excess dissipation due to surface roughness (specification in Ref. [33], Appendix A4), we have investigated this problem in isotopically pure ^{4}He cooled to millikelvin temperatures. We discovered an even more complex scenario involving *three* different critical velocities of hydrodynamic origin, see Ref. [39] in Appendix A3 for details. Our interpretation of this

observation, supported by order of magnitude estimates, confirmed the previously observed first critical velocity, and our results were consistent with the hypothesis of vortex loops spreading on the oscillator surface. As we detected no extra damping above the first critical velocity, at least up to the limits given by the sensitivity of the tuning forks used, our results support the observations in Refs. [22, 38] rather than those reported in Refs. [35–37]. We note that with an effective mass of 1.6×10^{-8} kg, resonant linewidth of 8 mHz and a quality factor of $Q = 8 \times 10^5$ at the lowest temperatures, the tuning forks used here are far more sensitive to the production of quantized vortices than any of the devices used previously. We are therefore left to conclude that the extra damping observed in some of the previous work [35–37] may have been due to effects such as surface roughness or acoustic dissipation (see the following Section 2.3 for more details).

The second critical velocity we observed, marked by a steep increase in the drag force, was then associated the with the production of vortex rings by the self-reconnections of vortex loops pinned on the surface of the oscillator [11, 18, 40]. The vortex rings would carry momentum and energy away from the oscillator (thus providing the extra damping), and eventually collide with each other and form a vortex tangle. However, the drag coefficients observed at this point were still significantly below those expected in a classical fluid in the same range of velocities, of order unity, which were also experimentally observed with the same tuning fork in ^{4}He at higher temperatures, see, e.g., Ref. [34] in Appendix A1). This situation would correspond to a random (unpolarized) tangle of quantized vortices, lacking any larger structures typical of classical turbulent flow. Finally, above the third critical velocity, the quantum turbulence started to mimic its classical counterpart, in the sense that the value of the drag coefficient approached that observed under similar conditions in a classical fluid (normal helium). This effect can be explained by large flow structures developing in the wake of the oscillator during each swing, requiring partial polarization of the tangle of quantized vortices, see again Ref. [39] in Appendix A2 for further details.

2.3 Acoustic Emission by Oscillators in ^{4}He

It is a well known fact that any object moving with finite acceleration inside a compressible fluid will lose energy by emitting sound waves [16]. This, in principle, introduces an additional dissipation mechanism acting alongside viscous forces or turbulent drag, but the acoustic contribution is usually sufficiently small to be neglected in most practical applications. In a statistically steady flow past a given bluff body, acceleration of the fluid usually occurs only in a (periodic) array of vortices shed from the boundary layer of said object (Kármán vortex street), as investigated in detail by Strouhal [41], or via turbulent fluctuations [42, 43]. In this case, acoustic emission may usually be neglected, although (ultra-)sonic investigations of vorticity within turbulent flow have been described [44] and in common use for some time [45].

However, in oscillatory flows, the situation may be very different. Depending on the oscillator geometry and frequency, acoustic losses may easily compete with viscous drag forces, especially in easily compressible fluids such as air or other gases. At first sight, it may therefore seem surprising to discuss the importance of acoustic emission in liquid (or superfluid) helium, as liquids are usually consid-

ered nearly incompressible for most practical purposes. However, the best easily appreciable quantity characterising the compressibility of a fluid is perhaps the sound velocity c itself, linked to the inverse adiabatic compressibility via:

$$c^2 = \left.\frac{\partial p}{\partial \rho}\right|_S , \tag{2.3}$$

where p is the fluid pressure, ρ its density, and the derivative is taken at constant entropy S, corresponding to the adiabatic propagation of the sound wave. In liquid and superfluid helium, sound velocity (at saturated vapour pressure) ranges from 181.6 ms^{-1} at the boiling point (4.2 K) to 238.2 ms^{-1} in the zero temperature limit [46], which is less than the sound velocity in dry air, $\approx$ 343 ms^{-1} under ambient conditions. In reality, liquid helium is therefore *more compressible* than dry air at room temperature and sound emission is expected to be important.

Indeed, the importance of sound emission as a parasitic effect in investigations of superfluids and quantum turbulence cannot be understated, since any viscous drag is markedly suppressed in superfluids, especially as the density of the normal component drops with decreasing temperature [46]. Ultimately, acoustic emission may be the dominant dissipative process in the linear regime at very low temperatures, determining the sensitivity of any device used to detect the first quantized vortices appearing at the turbulent instability, see, e.g., Ref. [47] for discussion of nanomechanical beams in ^{4}He.

It is therefore of prime importance to understand acoustic emission due to the typical sensors used in quantum turbulence research, and develop ways to eliminate or suppress its effect. Here, we will discuss two types of sensors, namely the quartz tuning fork, and a suspended beam, and we will limit our discussion to superfluid ^{4}He. The tell-tale sign of acoustic emission, distinguishing it from viscous damping in experimental data is its steep frequency dependence. While viscous dissipation $\dot{E}_{\mathrm{visc}}$ scales with the angular frequency as $\dot{E}_{\mathrm{visc}} \propto \omega^{1/2}$ [27, 34], acoustic damping exhibits much higher exponents, varying from $\dot{E}_{\mathrm{ac}} \propto \omega^3$ obtained for an infinitely long oscillating cylinder (acoustic dipole) to $\dot{E}_{\mathrm{ac}} \propto \omega^6$ for a longitudinal quadrupolar source small in comparison with the sound wavelength, such as the tuning fork [48].

Acoustic emission by tuning forks in superfluid helium was first investigated by us in collaboration with the group from B. Verkin Institute in Kharkiv, and such a steep frequency dependence of the observed damping was indeed found, together with highly damped and distorted resonance peaks measured using high frequency commercial quartz tuning forks, see Ref. [32], Appendix A3. In the same work, three different models of acoustic emission by tuning forks were developed and compared favourably with the experimental data, while acoustic emission by other structures used for quantum turbulence research was discussed in detail as well. It was also found that the geometry and material of the enclosure of the oscillator may significantly reduce the observed acoustic damping, due to the reflection of sound waves, but, on the other hand, might introduce coupling between the mechanical resonance of the device and acoustic standing waves in the experimental volume, resulting in a steep increase in the device dissipation when its resonant frequency is close to one of the acoustic modes.

This investigation led directly to developments in sensor design, as the Lancaster University group has manufactured novel types of tuning fork sensors, with

adapted dimensions and resonant frequencies to either suppress or, on the other hand, study acoustic emission under controlled conditions, with minimum variation between the individual resonators. Systematic measurements of acoustic emission by tuning forks was then performed in close collaboration with the Lancaster group, see Ref. [33] in Appendix A4, confirming the previously proposed frequency dependencies predicted for tuning forks in Ref. [32], Appendix A3. It is worth to mention that as a result of this development, it was the new custom-made tuning forks that were used to perform the investigations of quantum turbulence discussed in the previous Sections 2.1 and 2.2, which was crucial for our analysis and interpretation, allowing us to discount most parasitic effects.

Modern developments in sensor design for superfluid revolve around the use of nanomechanical devices such as suspended nanobeams. While these devices are much smaller in size than any sensors used previously, their frequencies are significantly higher, often in the MHz range. Given their nature as acoustic dipolar sources, they exhibit a less steep frequency dependence than tuning forks, and we expect $\dot{E}_{\mathrm{ac}} \propto \omega^3$ if the beam is much longer than the wavelength at its frequency, or $\dot{E}_{\mathrm{ac}} \propto \omega^4$ in the opposite limiting case. Carefully designing the nanodevice geometry is of paramount importance, as demonstrated recently by the Lancaster group, which reported acoustic dissipation as the dominant dissipation mechanism at millikelvin temperatures in superfluid ^{4}He for their nanobeams resonating at MHz frequencies [47]. It is no surprise that nanomechanical devices of different geometries are already being developed, bringing the resonant frequency down to the kHz range [49].

Apart from the ordinary sound mode (a density wave, termed "first sound" in connection with superfluids), other sound modes exist in superfluid ^{4}He, such as a temperature wave ("second sound"), sound waves on a thin thin film of helium accompanied by quantum evaporation ("third sound"), or a wave of both density and temperature propagating in narrow, microscopically constricted areas ("fourth sound"). These are to a large extent irrelevant to the description of energy dissipation in oscillatory flows, perhaps with the exception of second sound, which may be generated at double the frequency of oscillation due to heating of the fluid and the oscillator surface caused by friction forces. While coupling to second sound resonances has already been reported [50], no evaluation of the related drag force due to second sound emission has been made and it remains to be seen whether this effect contributes to the total damping in an appreciable manner.

Another topic for future research in this area is the effect of acoustic emission in the superfluid phases of ^{3}He, as different sound modes exist (apart from first sound) in the fermionic superfluid than in the bosonic ^{4}He. At the moment of writing of this Thesis, the Prague Superfluidity group is submitting a proposal to the European Microkelvin Platform [51] to perform such investigations in ^{3}He-B together with our partners from Lancaster University.

2.4 Andreev Reflection of Excitations in ^{3}He-B

The rare isotope ^{3}He is a fermionic system and undergoes the superfluid transition at a significantly lower temperature than ^{4}He; its critical temperature T_{C} varies between 1 and 2 mK depending on the pressure. It has several superfluid phases, which occupy different parts of the phase diagram depending not only on

temperature and pressure, but also on the magnetic field, as ^{3}He atoms have a nuclear spin of 1/2 and a corresponding magnetic moment. Additionally, unlike electrons in superconductors, the Cooper pairs formed by ^{3}He atoms during the superfluid transition have a total spin of 1 (triplet state), and an angular momentum of 1 (p-wave pairing), as well. Hence, simply put, the physical description of superfluid ^{3}He is much richer and much more complex than that of ^{4}He, and is governed by spatial textures of parameters describing the orientation of the angular momentum and spin vectors. An introduction to the superfluidity in ^{3}He can be found, e.g., in Ref. [3].

The superfluid B phase (denoted ^{3}He-B) exists preferentially at low magnetic fields and low temperatures, and may be viewed as the closest to superfluid ^{4}He. It has an isotropic bandgap separating the ground state of the Cooper pairs of ^{3}He atoms from excitation bands, which have sharp minima at the Fermi momentum. Like in superfluid ^{4}He, a normal and a superfluid component may be postulated, with the normal component consisting of these thermal excitations. However, it is worth to point out that in ^{3}He-B, given its bandgap, the concentration of thermal excitations depends approximately exponentially on the temperature. Hence at low temperatures, the normal component becomes so dilute that it can be described as ballistically propagating thermal excitations [3]. Moreover, any device sensitive to momentum and energy exchange with the excitations may act, once calibrated, as an excellent thermometer. Historically, vibrating wires and tuning forks have been used for this purpose with outstanding performance [26, 52].

The existence of the sharp minima in the dispersion relation of the excitations has a profound consequence – a retro-reflection process becomes possible on defects within the superfluid, or even on gradients of the superfluid velocity field, in which the excitations exchange (practically) zero momentum with their surroundings. This is fully analogical to the reflection first described by Andreev in superconductors [53], and hence the same term is used to describe the process in superfluid ^{3}He. Andreev reflection of thermal excitations may occur [54], for example, in the close vicinity of quantized vortices (in ^{3}He the quantum of circulation is $\kappa_3 = h/(2m_3)$, where $2m_3$ is the mass of the Cooper pair). In consequence, quantized vortices may partially shield a given volume from an excitation flux coming from the surroundings, limiting the net heat transfer, an effect which is easily measured using sensitive thermometers, such as wires or quartz tuning forks.

Therefore, an experimental study of this phenomenon, with the idea to exploit this property for measuring the density of quantized vortices in ^{3}He-B, was proposed together with the Helsinki low temperature group. To create a defined arrangement of quantized vortices, their rotating cryostat was used, capable of reaching angular velocities of 3 rad s^{-1}. Under suitable driving conditions, an equilibrium triangular grid of quantized vortices formed below the cell, and the thermalization time of a volume containing two tuning forks could be measured as a function of the angular velocity of rotation (corresponding to the density of quantized vortices). Of the two tuning forks, one was used as a heater (oscillating at high drives), and the other as a thermometer (at low drives). The results showed a dependence of the heat flux through the orifice of the cell on the angular velocity of rotation, as the heat flux was modified due to Andreev

reflection of thermal excitations on the array of quantized vortices below the cell. As expected, the change due to Andreev reflection was found to be linear with the density of quantized vortices until a certain value, above which screening effects became noticeable. For details, see the full Ref. [55] in Appendix A5.

This measurement formed the basis for further development, as it laid down the proof-of-principle for a quantized vortex imaging device, a "thermal excitation camera". Indeed, such a device was later developed at Lancaster University [56, 57], utilizing a 5x5 array of sensitive custom-made tuning forks, and its basic functionality was successfully demonstrated. Future plans involve replacing tuning forks with a multiplexed nanomechanical beam array, increasing substantially the spatial resolution and sensitivity of such a new imaging device.

3. Thermal Convection in Two-Phase Cryogenic Helium

3.1 Motivation

Convective flows widely occur as part of many natural phenomena, e.g., Earth's atmosphere, the Sun's convective zone, or within other types of stars. Additionally, they have significant practical importance in everyday applications such as ventilation and air conditioning, or in industrial heat exchangers. A model system that can be easily studied in laboratory conditions is Rayleigh-Bénard convection [58], when the heat transfer is measured between two typically circular plates separated by a vertical gap of size H in the gravitational field g. The space between the plates is filled with the working fluid of density ρ. The most important parameter determining the properties of the convective flow is the Rayleigh number, $Ra = \beta\rho H^3 g\Delta T/(\nu\alpha)$, where β is the volume expansion coefficient, ΔT the temperature difference between the two plates, ν the kinematic viscosity and α the thermal diffusivity of the fluid.

Cryogenic helium vapour is an excellent medium for the studies of thermal convection [59, 60], as it offers extremely low values of both kinematic viscosity and thermal diffusivity, especially near the critical point at $T \simeq 5.2$ K, $p \simeq 2.26$ bar [61, 62]. Hence a relatively small setup with cryogenic helium allows reaching the same values of the control parameter Ra as a large installation using water or air. For this reason, the Prague group established collaboration with the Institute of Scientific Instrumentation in Brno, where such a setup [63] has been constructed.

3.2 Temperature Inversion and Precipitation in Two-Phase Convection

Here we will limit our discussion to a specific type of convective flow, where two phases of the same working fluid are present in the convection cell simultaneously. In our case, we will discuss two such systems, the first consisting of normal liquid helium and helium vapour (L/V system), while in the second the normal liquid phase has been replaced by the superfluid (S/V system). The details may be found in the Refs. [64, 65] attached in Appendices A6 and A7.

The convection setup [63] is operated in such a manner, that the bottom plate (made of high conductivity copper) is heated by a uniformly distributed resistive heater, to produce an elevated temperature compared to the top plate, which is cooled by a thermal link (via a separate heat exchanger chamber filled with helium vapour) to the liquid helium bath. In all standard Rayleigh-Bénard convection experiments, the temperature difference $\Delta T = T_\mathrm{B} - T_\mathrm{T}$, where T_B and T_T stand for the temperatures of the bottom and top plates, respectively, is positive, as expected from the heating/cooling arrangement of the two plates.

Surprisingly, during the two-phase convection experiments with the L/V system, a temperature inversion with respect to the direction of the heat flux was

observed, with the (heated) bottom plate showing a *lower temperature* than the (cooled) top plate, that is a negative ΔT. In other words, this corresponds to a heat flux from a colder body (bottom plate) to a hotter one (top plate). This effect appeared some time after the heater in the bottom plate was turned on, and lasted while there was liquid inside the cell. After checking for instrumental effects, an explanation needed to be found for this phenomenon, which might at the first sight seem to defy the laws of thermodynamics.

First of all, let us explain that the laws of thermodynamics are not broken in this system, as the traditional notion that heat flows from the hotter body to the colder one only applies to closed systems. In our case, heat enters and leaves the convection cell; we are therefore dealing with an open system. Nonetheless, the observed phenomenon posed an interesting challenge, with possible connections to atmospheric physics, and clearly deserved a detailed explanation. In short, it was found that nucleate boiling occurring at the lower plate can lead to bypassing the liquid phase as a thermal reservoir, carrying a part of the supplied heat directly to the vapour phase and hence to the top plate, while the lower plate remains cooled by the liquid. A detailed computer simulation of the thermodynamics of this system was performed, and a good agreement with experimental results was found. Both experimental and numerical results are described in detail in Ref. [64], Appendix A6.

The hypothesis of nucleate boiling being responsible for the temperature inversion was further tested experimentally in the S/V system, where, due to the extremely high heat conductivity of the superfluid phase (exceeding that of normal liquid helium $\approx 3 \times 10^6$ times), nucleate boiling is completely suppressed, as no hot spots for preferential bubble nucleation exist. Indeed, no temperature inversion was observed while the liquid helium was in superfluid state, but once the temperature was raised above the superfluid transition, the temperature inversion was recovered, see Ref. [65], Appendix A7.

As a point of interest, we mention that inside the 30 cm tall convection cell, condensation of helium vapour on the top plate caused a precipitation, a form of "helium rain", observed as extremely high "noise" on thermometers placed inside the cell volume within the vapour phase that were not in contact with any surfaces. The temperature readings exhibited rapid departures towards the value of the top plate temperature and back to the vapour temperature as the liquid helium droplets hit the thermometer or its leads, see again Ref. [64], Appendix A6. This observation brings hope that such a laboratory system, or a similar one containing more than one working fluid, could indeed be used in the future to model specific aspects of weather formation in the Earth's atmosphere.

4. Continuous Nuclear Demagnetization Refrigeration

In this Chapter we will discuss the predominantly technical development of a novel type of refrigerator capable of continually maintaining temperatures below 1 mK. This development was started during the author's post-doctoral stay at the Institut Néel in Grenoble, France, and to this day remains an active avenue of collaboration between the author and the Grenoble group. The author contributed to this effort on both the physics level and the technical level. The scientific contributions include mainly devising and performing numerical simulations of the thermodynamics of the chosen nuclear refrigerant ($PrNi_5$) and of the overall performance of the CNDR. The technical contributions include designing a platform for measurements of small (nΩ) resistances of high purity metals at low temperatures, performing said measurements in order to optimize the treatment of metals, helping to design the magnetic shielding for the superconducting solenoid, performing vibration measurements on the dilution refrigerator, measuring thermal conductances of aluminium heat switches as well as evaluating the thermal performance of a testing nuclear stage and the newly developed compact superconducting magnet.

As some specific technical details remain the intellectual property of the Institut Néel and cannot be published at this point, the reader is kindly asked to make their own qualified judgment of these specific aspects of development – most notably the material preparation techniques needed to obtain sufficiently low thermal resistances for the heat switches and linking elements. Nevertheless, a significant part of the work discussed here has already been published [66–68] and is included in Appendices A8, A9, and A10 for convenience.

4.1 Motivation

Experimental investigations in low temperature physics would not be possible without the technology necessary to reach and accurately measure low temperatures. At the beginning of low temperature physics stands the event of the first liquefaction of helium [69], accomplished by H. K Onnes in Leiden in 1908. As the technology progressed, lower temperatures became available and new phenomena were gradually discovered, e.g., superfluidity of ^{4}He [70, 71], the fermionic superfluid ^{3}He [72], and more recently topological superfluid phases of ^{3}He under nanoscale confinement [4, 5].

Today, the most powerful refrigerators are based on dilution refrigeration systems, precooled either with liquid helium or a pulse tube cooler. The dilution refrigerator alone reaches temperatures of order units of millikelvins (typically between 5 and 10 mK). This base temperature then becomes a starting point for further refrigeration using either the Pomeranchuk effect in ^{3}He, or more commonly, nuclear demagnetization techniques [73]. The principle of operation of a nuclear demagnetization refrigerator is relatively simple. A suitable nuclear refrigerant is chosen – a material with nonzero nuclear spin and favourable thermal and magnetic properties, typical examples include copper and $PrNi_5$. Such

a material fashioned into a nuclear stage, which is then precooled by the dilution refrigerator to millikelvin temperatures while in a large external magnetic field of several tesla, necessary to align the nuclear magnetic moments and remove additional entropy from the system. The nuclear stage is then thermally decoupled from the dilution refrigerator, usually by means of a superconducting heat switch, and upon reduction of the external magnetic field, produces additional cooling, as the magnetic moments lose their alignment and absorb energy from their surroundings to increase their entropy [73].

The final temperature is determined by the material of choice, the initial temperature, the initial and final values of the magnetic field and the external heat leak into the nuclear stage. However, once the magnetic field is reduced to its final value, no further cooling is possible and the entire setup slowly warms up at the rate determined by the heat leak and the heat capacity of the nuclear stage. Copper stages can produce temperatures below 100 μK, with carefully designed double stage setups reaching the record values of units of μK [74]. However, they do not retain these temperatures for a very long time – usually approximately one or a few days below 0.5 mK are possible. $PrNi_5$ stages cannot reach such low temperatures, due to spontaneous ordering of the nuclear spins close to 0.4 mK, however, have a much higher heat capacity and thus perform better under more severe heat loads. They typically allow remaining near 1 mK for approximately one week, depending on the external heat leak [73].

As thermalization times for non-conducting materials (say, silicon chips with nanomechanical or optomechanical devices) diverge as one approaches absolute zero [73], the experimental time scales offered by present demagnetization setups have become insufficient. With such devices, thermal decoupling is routinely observed already above the millikelvin level (see Ref. [67], Appendix A10 as a broad example). To advance ultra-low temperature research, it is therefore of prime interest to design and construct a refrigerator capable of maintaining sub-millikelvin temperatures indefinitely, a Continuous Nuclear Demagnetization Refrigerator (CNDR).

4.2 Design and Development

To ensure that CNDR setups would see a widespread use, it is necessary to develop them for the most widely used type of dilution refrigerator – cryogen free system precooled by a pulse tube cooler. This brings additional challenges, as the external heat leak will necessarily contain contributions from the vibrations of the dilution refrigerator, which always remains weakly coupled to the pulse tube motor, despite significant efforts to suppress the transfer of vibrations. Practically, two main designs of the CNDR may be considered – the parallel and the serial configuration of two independent demagnetization stages connected via superconducting heat switches. The performance of the CNDR, and the minimum temperature it will be able to maintain will be ultimately determined by the design choices and by the quality of the thermal links in critical parts of the setup. As two independent demagnetization stages, each with its own dedicated superconducting solenoid, have to be fitted to a single dilution refrigerator, compactness and magnetic shielding represent important issues as well. We note that for electronic demagnetization refrigeration at slightly higher temperatures, the

parallel design seems to be the better choice in terms of raw cooling power, while the series design provides a much better final temperature stability [75].

The first design decision to be made is the choice of the nuclear refrigerant. In the end, $PrNi_5$ was chosen, due to its large heat capacity (and cooling power) per unit volume [73], and lower initial magnetic fields required, allowing us to downscale the superconducting solenoids (together with their 8 mm thick soft iron shielding) to a cylinder of diameter 54 mm and height 142 mm, while allowing for a maximum magnetic field of 2.5 T in the bore of diameter 22 mm. The solenoid design will be published once in final form.

To better understand the limitations of both serial and parallel versions of CNDR, numerical simulations have been performed, modeling the behaviour of the nuclear refrigerant, and the heat transfer through all the connecting elements including silver/copper wires and aluminium heat switches. In this task, modeling the thermodynamics of $PrNi_5$ was particularly challenging, because a straightforward implementation of the paramagnetic model does not describe the spontaneous ordering of spins at 0.4 mK. Using the Ising model with the interaction between the spins described by an effective field does not improve the results sufficiently, and in the end an empirical approach had to be used. The paramagnetic model was artificially modified in such a way as to obtain good agreement with experimental data on $PrNi_5$ near the ordering temperature, while maintaining the valid paramagnetic description at higher temperatures.

The main results of the simulations are presented in Ref. [66], Appendix A8 in the form of dependence of the final temperature (the maximum temperature during a stable cycle of the CNDR) on the external heat leak imposed on the sample space. It is clearly shown that the serial CNDR requires an extremely low thermal resistance of the second heat switch and attached wires connecting to both demagnetization stages. Using the Wiedemann-Franz law, the thermal resistance has to fall below the equivalent electrical resistance of 150 nΩ in order to be able to maintain temperatures below 1 mK under a moderate heat leak of 20 nW (expected on a dry dilution refrigerator). While the parallel design partly lifts this stringent requirement, see Fig. 4.1, very low thermal resistances of the two heat switches (and attached wires) connecting to the sample space are still necessary, with values close to 500 nΩ needed under the same conditions. This comes, however, at the cost of dealing with a more complex system – four superconducting heat switches are required instead of two used in the serial design.

The requirements for extremely low thermal resistance (in both design versions) mean that both bulk resistivity and interfacial contact resistances have to be minimised for any materials used. To this end, systematic measurements of high purity metals were undertaken and, eventually, sufficient values of the RRR (residual resistivity ratio) were obtained for particular treatments of 6N aluminium (heat switch material) and 5N copper (linking elements in the form of wires). Since typical resistances of order 100 nΩ were reported previously for pressed contacts [76], we devoted additional effort to optimizing them as well, and we found significant reduction in copper-aluminium pressed contact resistance using a specific preparation technique, which partly breaks the oxide layer on the aluminium and allows reaching contact resistances as low as 13 nΩ on an area $\approx$3 cm^2. The resistance was found to be stable on the time scale of one month.

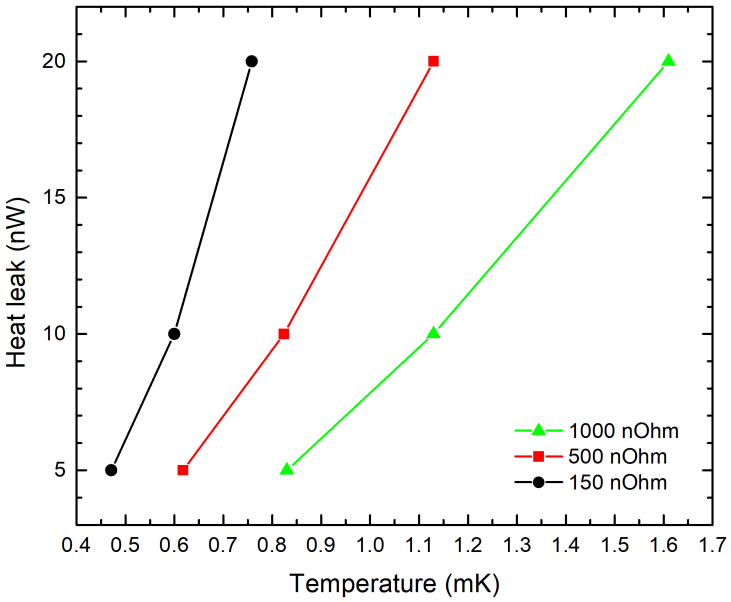

Figure 4.1: New, so far unpublished results on the final temperature versus heat leak for the parallel CNDR at the resistances of the thermal links, consisting of a heat switch and connecting wires, as indicated. Compare with Fig. 4 in Ref. [66], Appendix A8. The parallel CNDR allows reaching temperatures near 1 mK even with a resistance of the heat switch (and links) close to 500 nΩ.

The techniques used and the resistance measurements will be published in due course.

Additional efforts were devoted also to measuring the vibration levels on a pulse tube cooled dilution refrigerator in an effort to find adjustments and modifications which may suppress the associated heat leak. The results are published in Ref. [68], Appendix A9. Significant thought was also given to design and manufacture of the superconducting solenoid, its soft iron shield, and suitable thermal anchoring. The properties of the magnet have already been validated experimentally, and specific suggestions towards powering and filtering the magnet leads have been implemented.

At the time of writing this Thesis, the design and material preparation issues have been mostly dealt with, and what remains to be done is the actual construction and thorough evaluation of the performance of a two stage setup in parallel and/or serial configuration. Additional issues that will likely have to be addressed include an improvement of thermal shielding of the entire CNDR setup and possibly a better thermalization of the solenoids. At this stage we hope to complete all tests within the year 2020.

Bibliography

[1] I. M. Khalatnikov. *Introduction to the Theory of Superfluidity.* Benjamine, New York, 1965.

[2] D. R. Tilley and J. Tilley. *Superfluidity and Superconductivity.* Adam Hilger Ltd., 2 edition, 1986.

[3] D. Vollhardt and P. Wolfle. *The Superfluid Phases of Helium 3.* Dover Books on Physics. Dover Publications, 2013.

[4] L. V. Levitin, R. G. Bennett, A. Casey, B. Cowan, J. Saunders, D. Drung, Th. Schurig, and J. M. Parpia. Phase Diagram of the Topological Superfluid He-3 Confined in a Nanoscale Slab Geometry. *Science*, 340(6134):841–844, 2013.

[5] Lev V. Levitin, Ben Yager, Laura Sumner, Brian Cowan, Andrew J. Casey, John Saunders, Nikolay Zhelev, Robert G. Bennett, and Jeevak M. Parpia. Evidence for a Spatially Modulated Superfluid Phase of He-3 under Confinement. *Phys. Rev. Lett.*, 122(8), 2019.

[6] V. V. Zavjalov, S. Autti, V. B. Eltsov, P. J. Heikkinen, and G. E. Volovik. Light Higgs channel of the resonant decay of magnon condensate in superfluid He-3-B. *Nature Communications*, 7, 2016.

[7] J. T. Makinen, V. V. Dmitriev, J. Nissinen, J. Rysti, G. E. Volovik, A. N. Yudin, K. Zhang, and V. B. Eltsov. Half-quantum vortices and walls bounded by strings in the polar-distorted phases of topological superfluid He-3. *Nature Communications*, 10, 2019.

[8] Carlo F. Barenghi, Ladislav Skrbek, and Katepalli R. Sreenivasan. Introduction to quantum turbulence. *Proc. Nat. Acad. Sci. USA*, 111(1):4647–4652, 2014.

[9] Victor S. L'vov, Ladislav Skrbek, and Katepalli R. Sreenivasan. Viscosity of liquid He-4 and quantum of circulation: Are they related? *Phys. Fluids*, 26(4), 2014.

[10] L. D. Landau. On the Theory of Superfluidity. *Physical Review*, 75(5):884–885, 1949.

[11] William F. Vinen and Ladislav Skrbek. Quantum turbulence generated by oscillating structures. *Proc. Nat. Acad. Sci. USA*, 111(1):4699–4706, 2014.

[12] E. Varga, S. Babuin, and L. Skrbek. Second-sound studies of coflow and counterflow of superfluid He-4 in channels. *Phys. Fluids*, 27(6), 2015.

[13] Shaun Neil Fisher, Martin James Jackson, Yuri A. Sergeev, and Viktor Tsepelin. Andreev reflection, a tool to investigate vortex dynamics and quantum turbulence in He-3-B. *Proc. Nat. Acad. Sci. USA*, 111(1):4659–4666, 2014.

[14] Wei Guo, Marco La Mantia, Daniel P. Lathrop, and Steven W. Van Sciver. Visualization of two-fluid flows of superfluid helium-4. *Proc. Nat. Acad. Sci. USA*, 111(1):4653–4658, 2014.

[15] P. Svancara, P. Hrubcova, M. Rotter, and M. La Mantia. Visualization study of thermal counterflow of superfluid helium in the proximity of the heat source by using solid deuterium hydride particles. *Phys. Rev. Fluids*, 3(11), 2018.

[16] L.D. Landau and E.M. Lifshitz. *Fluid Mechanics*. Number sv. 6. Elsevier Science, 1987.

[17] K.W. Schwarz. Critical Velocity for a Self-Sustaining Vortex Tangle in Superfluid-Helium. *Phys. Rev. Lett.*, 50(5):364–367, 1983.

[18] R. Hanninen and W. Schoepe. Universal Onset of Quantum Turbulence in Oscillating Flows and Crossover to Steady Flows. *J. Low Temp. Phys.*, 158(3-4):410–414, 2010.

[19] R. J. Donnelly and A. C. Hollis Hallett. Periodic Boundary Layer Experiments in Liquid Helium. *Annals of Physics*, 3(3):320–345, 1958.

[20] A. M. Guénault, V. Keith, C. J. Kennedy, S. G. Mussett, and G. R. Picket. The Mechanical Behavior of a Vibrating Wire in Superfluid 3He-B in the Ballistic Limit. *J. Low Temp. Phys.*, 62(5-6):511–523, 1986.

[21] M. Morishita, T. Kuroda, A. Sawada, and T. Satoh. Mean Free Path Effects in Superfluid 4He. *J. Low Temp. Phys.*, 76(5-6):387, 1989.

[22] H. A. Nichol, L. Skrbek, P. C. Hendry, and P. V. E. McClintock. Flow of HeII due to an oscillating grid in the low-temperature limit. *Phys. Rev. Lett.*, 92(24), 2004.

[23] D. I. Bradley, S. N. Fisher, A. M. Guenault, R. P. Haley, Mukesh Kumar, C. R. Lawson, Roch Schanen, P. V. E. McClintock, Lydia Munday, G. R. Pickett, Malcolm Poole, V. Tsepelin, and Paul Williams. Turbulent drag on a low-frequency vibrating grid in superfluid He-4 at very low temperatures. *Phys. Rev. B*, 85(22), 2012.

[24] J. Jager, B. Schuderer, and W. Schoepe. Turbulent and Laminar Drag of Superfluid Helium on an Oscillating Microsphere. *Phys. Rev. Lett.*, 74(4):566–569, 1995.

[25] W. Schoepe. Fluctuations and stability of superfluid turbulence at mK temperatures. *Phys. Rev. Lett.*, 92(9), 2004.

[26] R. Blaauwgeers, M. Blažková, M. Človečko, V. B. Eltsov, R. de Graaf, J. Hosio, M. Krusius, D. Schmoranzer, W. Schoepe, L. Skrbek, P. Skyba, R. E. Solntsev, and D. E. Zmeev. Quartz tuning fork: Thermometer, pressure- and viscometer for helium liquids. *J. Low Temp. Phys.*, 146(5-6):537–562, 2007.

[27] M. Blažková, D. Schmoranzer, and L. Skrbek. Transition from laminar to turbulent drag in flow due to a vibrating quartz fork. *Phys. Rev. E*, 75(2, Part 2), 2007.

[28] M. Blažková, D. Schmoranzer, L. Skrbek, and W. F. Vinen. Generation of turbulence by vibrating forks and other structures in superfluid He-4. *Phys. Rev. B*, 79(5), 2009.

[29] M. Blažková, D. Schmoranzer, and L. Skrbek. On cavitation in liquid helium in a flow due to a vibrating quartz fork. *Low Temp. Phys.*, 34(4-5):298–307, 2008.

[30] M. Blažková, T. V. Chagovets, M. Rotter, D. Schmoranzer, and L. Skrbek. Cavitation in liquid helium observed in a flow due to a vibrating quartz fork. *J. Low Temp. Phys.*, 150(3-4):194–199, 2008.

[31] Daniel Duda, Patrik Svancara, Marco La Mantia, Milos Rotter, David Schmoranzer, Oleg Kolosov, and Ladislav Skrbek. Cavitation Bubbles Generated by Vibrating Quartz Tuning Fork in Liquid He-4 Close to the lambda-Transition. *J. Low Temp. Phys.*, 187(5-6):376–382, 2017.

[32] D. Schmoranzer, M. La Mantia, G. Sheshin, I. Gritsenko, A. Zadorozhko, M. Rotter, and L. Skrbek. Acoustic Emission by Quartz Tuning Forks and Other Oscillating Structures in Cryogenic 4He Fluids. *J. Low Temp. Phys.*, 163(5-6):317–344, 2011.

[33] D. I. Bradley, M. Clovecko, S. N. Fisher, D. Garg, E. Guise, R. P. Haley, O. Kolosov, G. R. Pickett, V. Tsepelin, D. Schmoranzer, and L. Skrbek. Crossover from hydrodynamic to acoustic drag on quartz tuning forks in normal and superfluid He-4. *Phys. Rev. B*, 85(1), 2012.

[34] D. Schmoranzer, M. J. Jackson, S. Midlik, M. Skyba, J. Bahyl, T. Skokankova, V Tsepelin, and L. Skrbek. Dynamical similarity and instabilities in high-Stokes-number oscillatory flows of superfluid helium. *Phys. Rev. B*, 99(5), 2019.

[35] D. I. Bradley, M. J. Fear, S. N. Fisher, A. M. Guenault, R. P. Haley, C. R. Lawson, P. V. E. McClintock, G. R. Pickett, R. Schanen, V. Tsepelin, and L. A. Wheatland. Transition to Turbulence for a Quartz Tuning Fork in Superfluid He-4. *J. Low Temp. Phys.*, 156(3-6):116–131, 2009.

[36] D. I. Bradley, S. N. Fisher, A. M. Guenault, R. P. Haley, V. Tsepelin, G. R. Pickett, and K. L. Zaki. The Transition to Turbulent Drag for a Cylinder Oscillating in Superfluid He-4: A Comparison of Quantum and Classical Behavior. *J. Low Temp. Phys.*, 154(3-4):97–116, 2009.

[37] Deepak Garg, V. B. Efimov, M. Giltrow, P. V. E. McClintock, L. Skrbek, and W. F. Vinen. Behavior of quartz forks oscillating in isotopically pure He-4 in the T -> 0 limit. *Phys. Rev. B*, 85(14), 2012.

[38] H. A. Nichol, L. Skrbek, P. C. Hendry, and P. V. E. McClintock. Experimental investigation of the macroscopic flow of HeII due to an oscillating grid in the zero temperature limit. *Phys. Rev. E*, 70(5, Part 2), 2004.

[39] D. Schmoranzer, M. J. Jackson, V. Tsepelin, M. Poole, A. J. Woods, M. Clovecko, and L. Skrbek. Multiple critical velocities in oscillatory flow of superfluid He-4 due to quartz tuning forks. *Phys. Rev. B*, 94(21), 2016.

[40] W. F. Vinen, L. Skrbek, and H. A. Nichol. The nucleation of superfluid turbulence at very low temperatures by flow through a grid. *J. Low Temp. Phys.*, 135(5-6):423–445, 2004.

[41] V. Strouhal. Ueber eine besondere art der tonerregung. *Annalen der Physik*, 241(10):216–251, 1878.

[42] M.J. Lighthill. On Sound Generated Aerodynamically. 2. Turbulence as a Source of Sound. *Proc. Roy. Soc. London Series A-Math. and Phys. Sciences*, 222(1148):1–32, 1954.

[43] H. Lamb. *Hydrodynamics*. Dover Books on Physics. Dover publications, 1945.

[44] R.H. Kraichnan. The Scattering of Sound in a Turbulent Medium. *J. Acoustical Society of America*, 25(6):1096–1104, 1953.

[45] F. Lund and C. Rojas. Ultrasound as a Probe of Turbulence. *Physica D*, 37(1-3):508–514, 1989.

[46] R. J. Donnelly and C. F. Barenghi. The observed properties of liquid helium at the saturated vapor pressure. *J. Phys. Chem. Reference Data*, 27(6):1217–1274, 1998.

[47] A. M. Guenault, A. Guthrie, R. P. Haley, S. Kafanov, Yu A. Pashkin, G. R. Pickett, M. Poole, R. Schanen, V Tsepelin, D. E. Zmeev, E. Collin, O. Maillet, and R. Gazizulin. Probing superfluid He-4 with high-frequency nanomechanical resonators down to millikelvin temperatures. *Phys. Rev. B*, 100(2), 2019.

[48] R. M. Sillitto. Angular Distribution of the Acoustic Radiation from a Tuning Fork. *American J. Phys.*, 34(8):639–644, 1966.

[49] T. Kamppinen and V. B. Eltsov. Nanomechanical Resonators for Cryogenic Research. *J. Low Temp. Phys.*, 196(1-2):283–292, 2019.

[50] E. Pentti, J. Rysti, A. Salmela, A. Sebedash, and J. Tuoriniemi. Studies on Helium Liquids by Vibrating Wires and Quartz Tuning Forks. *J. Low Temp. Phys.*, 165(3-4):132–165, 2011.

[51] George Pickett and Christian Enss. The European Microkelvin Platform. *Nature Reviews Materials*, 3(3), 2018.

[52] C. B. Winkelmann, E. Collin, Y. M. Bunkov, and H. Godfrin. Vibrating wire thermometry in superfluid He-3. *J. Low Temp. Phys.*, 135(1-2):3–14, 2004. Conference on Pushing Physics at Low Temperatures held in Honour of Francisco LaCruz, San Carlos Bariloche, Argentina, Sep 25-26, 2003.

[53] A. F. Andreev. The Thermal Conductivity of the Intermediate State in Superconductors. *Soviet Physics JETP-USSR*, 19(5):1228–1231, 1964.

[54] M. P. Enrico, S. N. Fisher, A. M. Guénault, G. R. Pickett, and K. Torizuka. Direct Observation of the Andreev Reflection of a Beam of Excitations in Superfluid 3He-B. *Phys. Rev. Lett.*, 70(12):1846–1849, 1993.

[55] J. J. Hosio, V. B. Eltsov, R. de Graaf, M. Krusius, J. Makinen, and D. Schmoranzer. Propagation of thermal excitations in a cluster of vortices in superfluid He-3-B. *Phys. Rev. B*, 84(22), 2011.

[56] A. W. Baggaley, V. Tsepelin, C. F. Barenghi, S. N. Fisher, G. R. Pickett, Y. A. Sergeev, and N. Suramlishvili. Visualizing Pure Quantum Turbulence in Superfluid He-3: Andreev Reflection and its Spectral Properties. *Phys. Rev. Lett.*, 115(1), 2015.

[57] V. Tsepelin, A. W. Baggaley, Y. A. Sergeev, C. F. Barenghi, S. N. Fisher, G. R. Pickett, M. J. Jackson, and N. Suramlishvili. Visualization of quantum turbulence in superfluid He-3-B: Combined numerical and experimental study of Andreev reflection. *Phys. Rev. B*, 96(5), 2017.

[58] G. Alexander. *Rayleigh-benard Convection: Structures And Dynamics*. Advanced Series In Nonlinear Dynamics. World Scientific Publishing Company, 1998.

[59] P. Urban, V. Musilova, and L. Skrbek. Efficiency of Heat Transfer in Turbulent Rayleigh-Benard Convection. *Phys. Rev. Lett.*, 107(1), 2011.

[60] P. Urban, P. Hanzelka, T. Kralik, V. Musilova, A. Srnka, and L. Skrbek. Effect of Boundary Layers Asymmetry on Heat Transfer Efficiency in Turbulent Rayleigh-Benard Convection at Very High Rayleigh Numbers (vol 109, 154301, 2012). *Phys. Rev. Lett.*, 109(18), 2012.

[61] S.W. Van Sciver. *Helium Cryogenics*. International Cryogenics Monograph Series. Springer US, 1986.

[62] V. D. Arp and R. D. McCarty. The properties of critical helium gass. Technical report, 1998. Tech. Rep., U. of Oregon.

[63] P. Urban, P. Hanzelka, T. Kralik, V. Musilova, L. Skrbek, and A. Srnka. Helium cryostat for experimental study of natural turbulent convection. *Rev. Sci. Instr.*, 81(8), 2010.

[64] P. Urban, D. Schmoranzer, P. Hanzelka, K. R. Sreenivasan, and L. Skrbek. Anomalous heat transport and condensation in convection of cryogenic helium. *Proc. Nat. Acad. Sci. of the USA*, 110(20):8036–8039, 2013.

[65] P. Urban, P. Hanzelka, I Vlcek, D. Schmoranzer, and L. Skrbek. Convective heat transport in two-phase superfluid/vapor He-4 system. *Liw Temp. Phys.*, 44(10):1001–1004, 2018.

[66] David Schmoranzer, Rasul Gazizulin, Sebastien Triqueneaux, Eddy Collin, and Andrew Fefferman. Development of a Sub-mK Continuous Nuclear Demagnetization Refrigerator. *J. Low Temp. Phys.*, 196(1-2):261–267, 2019.

[67] David Schmoranzer, Sumit Kumar, Annina Luck, Eddy Collin, Xiao Liu, Thomas Metcalf, Glenn Jernigan, and Andrew Fefferman. Observations on Thermal Coupling of Silicon Oscillators in Cryogen-Free Dilution Refrigerators. *J. Low Temp. Phys.*, 196(1-2):268–274, 2019.

[68] D. Schmoranzer, A. Luck, E. Collin, and A. Fefferman. Cryogenic broadband vibration measurement on a cryogen-free dilution refrigerator. *Cryogenics*, 98:102–106, 2019.

[69] H. K. Onnes. The condensation of helium. *Nature*, 77:559, 1908.

[70] P. Kapitza. Viscosity of liquid helium below the gimel-point. *Nature*, 141:74, 1938.

[71] J. F. Allen and A. D. Misener. Flow of liquid helium II. *Nature*, 141:75, 1938.

[72] D. D. Osheroff, W. J. Gully, R. C. Richardson, and D. M. Lee. New Magnetic Phenomena in Liquid He-3 Below 3 mK. *Phys. Rev. Lett.*, 29(4):920, 1972.

[73] F. Pobell. *Matter and Methods at Low Temperatures*. Springer-Verlag, Berlin, 1992.

[74] K. Gloos, P. Smeibidl, C. Kennedy, A. Singaas, P. Sekowski, R. M. Mueller, and F. Pobell. The Bayreuth Nuclear Demagnetization Refrigerator. *J. Low Temp. Phys.*, 73:101, 1988.

[75] Peter J. Shirron. Applications of the magnetocaloric effect in single-stage, multi-stage and continuous adiabatic demagnetization refrigerators. *Cryogenics*, 62:130–139, 2014.

[76] F. Blondelle, A. Sultan, E. Collin, and H. Godfrin. Electrical Conductance of Bolted Copper Joints for Cryogenic Applications. *J. Low Temp. Phys.*, 175(5-6):877–887, 2014.

Selected Publications

Table of Contents of the publications in the Appendix:

Appendix A1

D. Schmoranzer, M. J. Jackson, Š. Midlik, M. Skyba, J. Bahyl, T. Skokánková, V. Tsepelin, L. Skrbek, Dynamical similarity and instabilities in high-Stokes-number oscillatory flows of superfluid helium, *Phys. Rev. B* **99**, 054511 (2019), DOI: 10.1103/PhysRevB.99.054511.

This publication represents the culmination of a long term effort and summarizes the results of multiple experiments performed in the Prague Superfluidity Laboratory on the dissipation in high-Stokes-number oscillatory flows. The main result is the derivation and experimental confirmation of the Universal scaling relation obtained for the drag force originating from the normal component of superfluid helium in the laminar regime, at low velocity amplitudes. It is shown that the linear viscous drag force can be described by a single dimensionless parameter – the Donnelly number, which, moreover, fully determines the flow due to most oscillators used in our work (specifically, if their surface contains sharp corners or has roughness significant in comparison to the viscous penetration depth).

Additionally, the transition to turbulent drag in oscillatory flows around vibrating wires, tuning forks, double-paddle oscillators and a torsionally oscillating disc is analysed, with the aim to discriminate between turbulence triggered by a classical-like instability in the normal component or a Donnelly-Glaberson type instability in the superfluid component. It is shown experimentally that depending on the temperature and the geometry of the oscillator, either type of instability may occur first and we demonstrate their crossover due to the temperature dependence of the viscosity of the normal component.

Additional results include, for example, the correction of the theoretical description of the vibrating wire resonator (in previous work, the electrical and mechanical descriptions were not equivalent in terms of dissipated power). Another interesting aspect presented here for the first time is the excellent agreement between a numerical model for the forces acting on a rectangular beam (a tuning fork) and actual experimental data, with the error below 2%. This level of agreement is possible only thanks to careful lithographic preparation of the custom-made tuning forks, limiting their surface roughness to sub-micron scales, as well as advanced design aimed at minimizing losses due to acoustic emission.

DS contributed to this work on many different levels, as he was present for most of the experimental work and at the same time was the true driving force behind the derivation of the Universal scaling law and the interpretation of the turbulent instabilities. He was also solely responsible for the additional results discussed above as well as for writing the majority of the manuscript. The contributions of other co-authors are also very significant: MJJ took charge of several experiments with tuning forks and vibrating wires and of the subsequent data analysis, and helped with the preparation of the manuscript; ŠM was involved in the vibrating wire experiments; MS was in charge of the last series of measurements of the torsionally oscillating disc; JB performed the bulk of the measurements using custom-made tuning forks, TS was responsible for all torsional disc experiments (the last run together with MS), VT has kindly provided the custom-made tuning forks and helped with the preparation of the manuscript, as did LS, who offered his advice throughout the process.

Appendix A2

D. Schmoranzer, M. J. Jackson, V. Tsepelin, M. Poole, A. J. Woods, M. Človečko, L. Skrbek, Multiple critical velocities in oscillatory flow of superfluid 4He due to quartz tuning forks, *Phys. Rev. B* **94**, 214503 (2016), DOI: 10.1103/PhysRevB.94.214503.

In this work, we have investigated in detail the transition to turbulence in oscillatory flow of superfluid 4He due to quartz tuning forks, with emphasis on the behaviour of pure superfluid in the zero temperature limit. Measurements were performed partly in Prague and partly in Lancaster, focusing on the drag forces acting on two custom-made quartz tuning forks with fundamental resonances at 6.5 kHz and 55.5 kHz.

The main result presented here for the first time is the fact that in pure superfluid in the zero temperature limit, three distinct critical velocities of hydrodynamic origin were observed with both tuning forks. Moreover, the same results were observed in two different laboratories, ensuring the reproducibility of the effect.

The first critical velocity was associated with the growth and spreading of quantized vortex loops on the surface of the given oscillator, in partial agreement with previous work. Unlike some of the previous works we have seen no increase of the drag force at the first critical velocity, only a shift of the resonant frequency due to the additional hydrodynamic enhancement of the oscillator mass caused by the newly created vortex loops. In our previous work with tuning forks, this first critical velocity would have been missed, as we have used commercial tuning forks of worse quality and were limited to temperatures above 1 K, where it would be extremely difficult to observe.

At the second critical velocity, the drag coefficient (convenient non-dimensional representation of the drag force) increases sharply, marking the onset of extra energy dissipation due to quantum turbulence. Based upon comparison with previous work and order of magnitude estimates of both the critical velocity for the Donnelly-Glaberson instability and of the resulting vortex line density, we conjecture that this is due to vortex rings being emitted by the tuning fork, which later collide and form a tangle.

After the instability occurs at the second critical velocity and bulk quantum turbulence is produced, the drag coefficients remain still at least an order of magnitude below the levels observed with the same tuning forks in normal helium (or even in superfluid helium at sufficiently high temperatures above 1 K). The hydrodynamic explanation is that at this point, no large structures have developed in the wake of the tuning fork, which would appreciably change the flow field and hence the pressure drag. In this sense, quantum turbulence (between the second and third critical velocities) differs significantly from its classical counterpart, where such large scale vortical structures accompany the instability. However, above the third critical velocity, the observed drag coefficients start to shift towards the values found in classical fluids and we are hence left to conclude that polarization finally develops within the vortex tangle and, on length scales larger than the intervortex distance, quantum turbulence finally starts to mimic the classical one.

The Prague experiments were designed and performed jointly by DS and MJJ, while in Lancaster, it was MP, MČ and AJW who took the data. The initial version of the manuscript was prepared by MJJ, later reviewed by DS who, after processing all the data, added the full discussion of the three critical velocities and, at the suggestion of LS, incorporated the comparison with previous work. DS has also made the order of magnitude estimates in Appendix B, as requested by one of the reviewers prior to publication. VT has provided the custom-made tuning forks and, together with his co-workers, contributed the Lancaster data. Both VT and LS have helped with the writing of the manuscript.

Appendix A3

D. Schmoranzer, M. La Mantia, G. Sheshin, I. Gritsenko, A. Zadorozhko, M. Rotter, L. Skrbek, Acoustic emission by quartz tuning forks and other oscillating structures in cryogenic 4He fluids, *J. Low Temp. Phys.* **161**, 317–344 (2011), DOI: 10.1007/s10909-011-0353-1.

This publication represents the first experimental proof and a systematic theoretical description of acoustic emission by oscillators is superfluid helium, with focus on tuning forks. The motivation for this work was to explain effects observed with these sensitive oscillators that do not fit into the behaviour expected due to viscous drag or ballistic phonon drag at lower temperatures (below 0.6 K). These observations include spurious temporal variations of the resonant linewidth obtained at low drives Δf, which ought to be fully determined by the applicable viscous or ballistic drag forces. Further effects include slight changes in the scaling of the drag coefficient when the drive is ramped towards the critical value, sometimes resulting in the increase of the drag force, other times decreasing it for no obvious reason.

First it was found that when using tuning forks of significantly higher resonance frequencies than before, their resonance curves obtained in helium gas, liquid or superfluid phases no longer conform to a single Lorentzian peak, but instead, multiple distorted peaks appear. Furthermore, the frequency scaling of the observed damping, expressed in terms of Δf, did not follow the expectations for viscous drag $\Delta f \propto f^{1/2}$. Instead, a much steeper power law dependence was observed, with the exponent between 5 and 6. Note that at lower temperatures, the ballistic drag is expected to be frequency-independent.

This result prompted further work, and additional experiments were performed in Prague and Kharkiv (Ukraine) to elucidate this effect. Simultaneously, three theoretical models of acoustic emission by tuning forks were worked out, including both two- and three-dimensional treatments which may be considered as limiting cases, depending on the ratio of the sound wavelength to the length of the tines of the tuning fork. In the three-dimensional case, the tuning fork was modeled as a linear acoustic quadrupole. In one of the two-dimensional models, the same approach is used, while in the other, the fork is treated as two parallel (infinitely long) cylinders oscillating in anti-phase. The models compared favourably with the experiments, once acoustic resonances of the experimental volume and sound reflection on solid walls were taken into account, but the results were insufficient to reliably distinguish which model works best.

Further proof linking the observations with acoustic emission was given by measuring the same resonant spectra under different conditions (temperature, pressure), if the sound velocity was constant. Additionally, an avoided level crossing with an acoustic resonance of the cell was demonstrated when measuring the tuning fork in helium gas. As the acoustic damping also depends steeply on the sound velocity, c, with $\Delta f \propto c^{-5}$ in the three-dimensional model of acoustic emission the same scenario could also be independently confirmed by varying the pressure inside the experimental cell between saturated vapour pressure ($c \simeq 240$ ms^{-}1) and 24 bar (approaching the solidification pressure of $\approx$25 bar). Indeed, at high pressure acoustic damping was significantly suppressed and the

dissipation was dominated by viscous drag under all conditions except where the acoustic contribution was enhanced by resonances within the experimental cell.

Finally, acoustic emission produced by other types of oscillators used previously in quantum turbulence research is discussed, such as oscillating spheres, vibrating wires, oscillating grids, or micromechanical systems. Simple suggestions are offered to help suppress acoustic damping in experiments with superfluid helium. This work has had profound impact on the future design and production of sensors for quantum turbulence research, as is demonstrated, e.g., in the following publication in Appendix A4, where custom-designed tuning fork arrays are tested, or in a more recent work on nanomechanical systems.

The Prague experiments were performed jointly by DS and MLM (and both took part in analysing the data), while the Kharkiv data were contributed by GS, IG, and AZ. MR helped with the preparation of the experimental setup, and both MLM and LS offered their advice and suggestions during the preparation of the manuscript. The initial idea and the mathematical models of acoustic emission are due to DS, who was also responsible for writing the manuscript.

Appendix A4

D. I. Bradley, M. Človečko, S. N. Fisher, D. Garg, E. Guise, R. P. Haley, O. Kolosov, G. R. Pickett, V. Tsepelin, D. Schmoranzer, L. Skrbek, Crossover from hydrodynamic to acoustic drag on quartz tuning forks in normal and superfluid 4He, *Phys. Rev. B* **85**, 014501 (2012), DOI: 10.1103/PhysRevB.85.014501.

This experimental part of this work originates predominantly from the Lancaster low temperature laboratory, and deals with the measurements performed with custom-designed tuning forks, of which several series were produced in order to either suppress, or study in greater detail the acoustic emission discussed in the previous publication in Appendix A3.

The series of the new tuning forks had a uniform cross-sections of their tines (90 x 75 μm^2), much smaller than commercial forks, which typically have several hundred micrometers in either direction. On the other hand, the tine length was varied to obtain different fundamental resonant frequencies, ranging between 6 kHz (low frequency designed to suppress acoustic effects) to 36 kHz. This time, the measurements were not restricted to the tuning fork fundamental resonances, in addition, the first overtone (second resonant mode) frequencies ranging from 40 kHz to 223 kHz were used as well. The surface of the new tuning forks was also of significantly better quality, with typical roughness on the scale of 1 μm, whereas commercial tuning forks usually had roughness at least one order of magnitude higher.

After the motion of the tuning forks was calibrated by both electrical and independent optical means, experiments in superfluid helium were performed. The results have shown a clear cross-over between viscous and acoustic damping, occurring near 150 kHz for the tuning forks used. In was also shown that the three-dimensional model of acoustic emission proposed in the previous publication in Appendix A3 agrees better with the results better than the two-dimensional models.

On the practical level, the results obtained at 1.5 K showed that if these tuning forks with frequencies below 40 kHz are used, acoustic emission will represent less than 1% of the total energy dissipation. As in superfluid ^{4}He the viscous drag reduces with falling temperature, and eventually becomes the phonon ballistic drag below 0.6 K, scaling with the temperature as T^4, the threshold frequency will have to be reduced if measurements are performed at very low temperatures of order 10 mK. This led naturally to the selection of the lowest frequency (6 kHz) tuning forks as the most sensitive probes of quantum turbulence, which were subsequently used to obtain the data in the publications in Appendices A1 and A2.

While most of the work was performed by our colleagues from Lancaster University (with LS taking part in some of the experiments), DS contributed by modifying the models of acoustic emission to describe the series of tuning forks of equal cross-section in simpler terms, and by working out the full mechanical model of the tine of the tuning fork. This model was based on the full dynamical treatment of the Euler-Bernoulli equation, and is presented in the Appendix, written mostly by DS, with the most important results shown in the main text. The fundamental result of this model is the value of the effective mass of the tine given as $m_{\mathrm{eff}} = 1/4\rho_q TWL$, where ρ_q is the density of quartz and T, W,

L are the thickness, width and length of the tine, respectively. Importantly, it was shown that m_{eff} remains constant for any resonant mode of the tuning fork, while the effective spring constant changes, following $k_{\text{eff}} = m_{\text{eff}}\omega_n^2$, with ω_n denoting the angular frequency corresponding to the n-th resonant mode. This differs significantly from the static approach used in previous work, which had assumed a fixed spring constant derived from the static deflection of the Euler-Bernoulli beam $k_{\text{stat}} = EWT^3/(4L^3)$, where E is Young's modulus of quartz. This had resulted in a *less precise* effective mass given as $m_{\text{eff}}^{(1)} = 0.2427\rho_q TWL$ for the first (fundamental) resonant mode and $m_{\text{eff}}^{(2)} = 0.00618\rho_q TWL$ for the second mode. While the static approach had worked reasonably well for the fundamental resonance, it would have failed catastrophically if used to describe any of the the higher resonant modes, such as the overtone used in this work.

Appendix A5

J. J. Hosio, V. B. Eltsov, R. de Graaf, M. Krusius, J. Mäkinen, D. Schmoranzer, Propagation of Thermal Excitations in a Cluster of Vortices in Superfluid 3He–B, *Phys. Rev. B* **84**, 224501 (2011), DOI: 10.1103/PhysRevB.84.224501.

This publication is based on the author's two visits in the Low Temperature Laboratory at Aalto University in Helsinki, and represents the initial study and validation of the Andreev reflection technique [54], which may be used, under certain conditions, to quantify the amount of vortex lines in a given sample of superfluid ^{3}He-B.

To verify this rather special measurement technique, a well-known configuration of quantized vortices had to be used, such as a rectilinear array of vortices, which represents the equilibrium state under steady rotation of the cryostat. Indeed, providing steady rotation up to several rad s^{-1}, while maintaining sub-mK temperatures using a dilution refrigerator fitted with a demagnetization stage, represents a considerable technical challenge, hence the choice of the Helsinki rotating cryostat for this work.

As Andreev reflection of thermal excitations by quantized vortices effectively limits the heat flux between two volumes in the same sample of helium, the experimental arrangement was such that a small quartz-glass cell with two separate volumes was inserted into the sample volume filled with ^{3}He-B. The volumes were separated from each other and from the sample space by small orifices, of the order of hundreds of microns in diameter. These tiny orifices prevented the penetration of quantized vortices filling the sample space into the cell itself. One of the two compartments within the cell ("fork volume") contained two tuning fork oscillators and was connected directly to the sample space. The second compartment ("NMR volume") was only connected to the fork volume, and was used for nuclear magnetic resonance measurements of the ^{3}He-B sample, which may reveal information on the textures of the order parameter, or detect quantized vortices, should any reach the interior of the cell.

The measurements consisted of closely monitoring the temperature of the first compartment, using one of the two tuning forks as a sensitive thermometer (operated at low drive, capable of resolving 0.2 μK on the background of $\approx$ 500 μK), while the other was used as a heater (at high drive). Upon switching the heater fork on/off, the temperature of the fork volume changed, with separate thermal relaxation processes occurring: i) between the fork volume and the NMR volume, and ii) between the fork volume and the sample space. While the former process was rather fast (due to the larger orifice between the two parts of the cell and the rather small NMR volume), the relaxation to the sample space took significantly longer and was the main process studied.

With the entire cryostat under rotation, thermal relaxation was monitored carefully using the thermometer tuning fork. The observed change in the thermal resistance of the orifice was found to depend linearly on the angular velocity of rotation. Simultaneously, numerical simulations of thermal excitation propagation in an array of quantized vortices were performed, taking into account the process of Andreev reflection. Good quantitative agreement was found between the experiment and the simulations, with the experimental reflection coefficient

slightly below the calculated one. Unfortunately, the noise in the experimental data precluded a firm conclusion as to whether screening effects were observed, which the simulation had shown reliably.

Most of the work was performed by our colleagues from Helsinki, but DS contributed to the preparation of the experimental cell (quartz glass, inner surface chemically polished to provide a smooth surface with roughness below 100 nm), its installation on the cryostat, and performed the analysis of the thermal relaxation processes using Matlab code. DS was also partly responsible for the pre-selection and preparation of the tuning fork resonators, as well as for experimental data acquisition, under the supervision and with the help of the members of the Helsinki Low Temperature Laboratory. Numerical simulations were performed independently by JM.

Appendix A6

P. Urban, D. Schmoranzer, P. Hanzelka, K. R. Sreenivasan, L. Skrbek, Anomalous heat transport and condensation in convection of cryogenic helium, *Proc. Nat. Acad. Sci. USA* **110**, 8036 (2013), DOI: 10.1073/pnas.1303996110.

In this work, heat flux against the temperature gradient in a Rayleigh-Bénard convection cell filled with liquid and gaseous helium was reported and analysed. The experimental cell, consisting of two highly conductive copper plates brazed to thin stainless steel walls, was made at the Institute of Scientific Instrumentation in Brno, CZ, and the experimental part of the work was performed there.

The cell was fitted with thermometers in the top and bottom plates, as well as additional four suspended thermometers located approximately in the middle of its height. At the beginning of the experiment, the liquid level was approximately in the middle of the cell. We had, therefore, independent temperature measurements from both plates as well as the liquid and vapour phases of helium. If the resistive heater in the *bottom* plate was switched on (at a moderate power of 2 W) and kept on for several minutes, the *top* plate, which is in fact cooled via a heat exchanger from the liquid helium bath, became hotter than the bottom plate. This effect was reproducible and lasted while there was a sufficient amount of liquid left in the cell.

This counter-intuitive and seemingly puzzling result is best understood in the framework of a simple thermal model, where the thermodynamic system (the entire cell) is divided into four sub-systems: the two plates, helium vapour and liquid helium. Each of the sub-systems is assumed in local thermodynamic equilibrium with a well defined temperature and the pressure is assumed constant in the entire cell (neglecting small variations due to hydrostatic and hydrodynamic effects). Heat and mass fluxes are calculated between the individual sub-systems taking into account phase transitions between the liquid and vapour phases.

When the temperature inversion occurred, it was the vapour phase that had the highest temperature of all the sub-systems. Therefore, a mechanism had to exist, by which energy produced by the bottom plate heater entered the vapour phase directly, bypassing the liquid. Such a mechanism was found and identified as *nucleate boiling* in the vicinity of the bottom plate. Liquid absorbed heat from the bottom plate and became vapour, increasing the energy of the vapour phase by the difference in enthalpies between the liquid and the vapour (+ additional heating to at least partly cover the temperature drop between the liquid and the bottom plate), at the same time increasing the overall pressure within the cell. This could work only if the newly created bubbles at the bottom plate did not have sufficient time to exchange heat and matter with the surrounding liquid, before reaching the vapour by upward buoyant motion. Additional phase transitions that needed to be described included evaporation/condensation at the liquid/vapour interface and, under certain conditions, condensation at the top plate as well.

To model such a complex system numerically, a semi-empirical approach had to be taken. For example, the temperature of the phase interface (determining the evaporation/condensation rates) was taken to be equal to the liquid temperature (this is habitual for similar calculations), as the liquid has a significantly

larger specific heat than the vapour phase. Nucleate boiling rate at the bottom plate was determined using empirical relations from existing literature. The condensation at the top plate was described in a similar fashion to the processes at the liquid/vapour interface, with the difference that only a one-way process was allowed. As a result, the model contained a significant number of adjustable parameters (heat exchange coefficients, phase transition rates) which were tuned to a large extent manually, but in the end managed to describe the overall situation very well, reproducing closely the time traces of *all four* temperatures that were obtained from the experiments, as well as the pressure. Additionally, the model correctly reproduced the observation of a "helium rain" inside the cell, as condensation at the top plate occurred when the top plate temperature reached the vapour/liquid equilibrium value determined by the cell pressure. The role of nucleate boiling in the temperature inversion was confirmed in a subsequent series of experiments detailed in the following publication in Appendix A7.

All of the experiments reported here were performed at the Institute of Scientific Instrumentation in Brno by PU, while PH contributed significantly to the cell design. LS, KRS and PU prepared most of the manuscript and figures. DS was responsible for the detailed explanation of the temperature inversion effect and for the numerical modeling of this system, including the related descriptions within the manuscript.

Appendix A7

P. Urban, P. Hanzelka, I. Vlček, D. Schmoranzer, L. Skrbek, Convective heat transport in two-phase superfluid/vapor 4He system, *Low Temp. Phys.* **44**, 1001 (2018), DOI: 10.1063/1.5055836.

This work continues the investigations reported in the previous publication in Appendix A6, and the experiments were also performed at the Institute of Scientific Instrumentation in Brno.

In short, the same type of two-phase convection experiment was repeated, where the normal liquid helium was replaced by the superfluid phase. The superfluid, having an extremely high heat conductivity (at least 3×10^6 higher than the normal liquid), efficiently suppresses any nucleate boiling at the lower plate, as it precludes the occurrence of any overheated spots in the vicinity of surface defects of the bottom plate. We note in passing that this extremely high heat conductivity is the result of the superfluid phase being able to support a special type of flow that does not exist in classical fluids – thermal counterflow. In thermal counterflow, the inviscid superfluid component and the viscous normal component (carrying heat and entropy) flow in opposite directions with zero net mass transfer. As counterflow is driven primarily by temperature gradients within the superfluid, this results in highly efficient mechanism of equilibrating the temperature within the entire volume occupied by the superfluid phase.

Assuming our previous interpretation that the temperature inversion is primarily due to nucleate boiling at the bottom plate was correct, no temperature inversion should occur in the superfluid/vapour system. With nucleate boiling out of the question in the superfluid/vapour system, the experiment was repeated and indeed no temperature inversion was found. In fact, the temperatures of all sub-systems followed nearly the same time dependence while the superfluid phase was present, meaning that the entire thermodynamical system (top and bottom plates + superfluid and vapour phases) was very close to thermal equilibrium (differences below 7 mK existed between the top and bottom plates at the highest heater power of 2.08 W). Once the temperature rose above the superfluid transition, the superfluid phase underwent the second order phase transition and became the normal liquid. Then, the bottom plate would overheat slightly above the liquid temperature and the scenario described in Appendix A6 would repeat itself.

DS contributed to this work mainly by the discussion of the role of thermal counterflow and the suppression of nucleate boiling at the bottom plate. The manuscript was mostly written by PU and LS. The setup designed by PH and modified by PU and IV was used, who were both also responsible for the experimental work.

Appendix A8

D. Schmoranzer, R. Gazizulin, S. Triqueneaux, E. Collin, A. Fefferman, Development of a Sub-mK Continuous Nuclear Demagnetization Refrigerator, *J. Low Temp. Phys.* **196**, 261–267 (2019), DOI: 10.1007/s10909-018-02128-9.

This publication reports the first steps of the development process of a novel type of ultra-low temperature cooler, the Continuous Nuclear Demagnetization Refrigerator (CNDR). This work was undertaken during the author's postdoctoral stay at the Institut Néel in Grenoble.

The paper is focused on the numerical simulations of the performance of a CNDR consisting of two nuclear stages connected in series (a parallel design is also possible and the results of similar simulations are currently being prepared for publication). The main question that these simulations tackle is the feasibility of continuous sub-mK operation of such a device with a given sample heat leak (up to 20 nW) and given thermal resistances of the aluminium heat switches and thermal links between all components of the system. Additional heat leaks such as eddy current heating during the manipulation of the magnetic fields on the nuclear stages, or vibrational heating were considered as well. As the CNDR was designed for operation on a so-called dry dilution refrigerator (precooled by a pulse-tube cryocooler rather than a liquid helium bath), the vibration levels on such a device became an important issue and were investigated separately, see Appendix A9.

In the series configuration, two nuclear stages are used, separated from the mixing chamber of a dilution refrigerator and from each other by superconducting heat switches. The first nuclear stage (cooled by the dilution refrigerator mixing chamber at relatively high magnetic fields) is used to extract the magnetization heat from the second stage as its magnetic field is ramped up before a new cooling cycle can be initiated. Under suitable conditions, this allows keeping the second stage and the connected sample space cooled below 1 mK continuously.

It was soon found from the simulations that the most important element in the entire setup is the thermal link between the first and second stage, and in order to support a thermal load of 20 nW on the sample space below 1 mK, its thermal resistance must be less than the equivalent electrical resistance of 150 nΩ according to the Wiedemann-Franz law. This is a rather stringent technological requirement and may represent the deciding factor in the choice between the series and parallel designs.

In order to correctly model the performance of the CNDR successfully, the magnetic entropy of the nuclear refrigerant $PrNi_5$ needed to be described correctly as a function of temperature and magnetic field. Unfortunately, simple physical models, such as paramagnetic nuclear spins, or the Ising model with and effective internal field were insufficient to correctly describe said properties close to the spontaneous ordering temperature of $PrNi_5$ near 0.4 mK. Hence, a close agreement with experimental values reported in the literature became our prime criterion of accuracy, and a phenomenological model of $PrNi_5$ entropy was developed, building heavily on the limiting paramagnetic behaviour, while trying to closely replicate the spontaneous ordering as observed by Kubota et al.

At the time of writing of this Thesis, all individual components of the CN-

DR have demonstrated the required properties, including the thermal resistances of the linking wires as well as boundary thermal resistances. To complete the development process, the nuclear stage design ought to be finalised, followed by the assembly and integral tests on a dry dilution refrigerator. The design and construction of the CNDR remain an active avenue of collaboration between the author and the Grenoble group.

The original decision to develop the CNDR came from the needs of the Grenoble ultra-low temperature group, as thermal decoupling of nanofabricated devices became a common issue on dilution refrigerators (for illustration, see Appendix A10) as well as nuclear demagnetization setups. Furthermore, continuous sub-mK refrigeration is a practical requirement of cooling a nanomechanical oscillator resonating near 100 MHz to its quantum mechanical ground state – thus making a highly interesting macroscopic quantum system that can be used advantageously to study, e.g., decoherence effects. Designs of the individual components of the CNDR were the result of the numerous discussions between all members of the group at the Institut Néel. Among other, DS was responsible for performing the numerical simulations, devising the thermodynamical model of $PrNi_5$ and for the writing of the manuscript.

Appendix A9

D. Schmoranzer, A. Luck, E. Collin, A. Fefferman, Cryogenic broadband vibration measurement on a cryogen-free dilution refrigerator, *Cryogenics* **98**, 102–106 (2019), DOI: 10.1016/j.cryogenics.2019.01.010.

This technical publication details the measurements performed at the Institut Néel in Grenoble concerning vibration levels of the dilution refrigerator BlueFors LD-400, precooled by the Cryomech PT-415RM cryocooler, with the aim of finding suitable precautions to minimize the impact of vibrations on sensitive low-temperature experiments performed on this refrigerator.

The work reported here represents a first attempt to measure the vibration levels not only at room temperature, but directly under cryogenic conditions. While this is an important advance in the area, it required making several compromises. First, the lowest temperatures had to be limited to the vicinity of 4 K or 5 K on the mixing chamber, as the accelerometers used dissipated a significant amount of heat. We are convinced that this does not represent any practical limitations, as the mechanical properties of the metallic parts of the dilution refrigerator no longer change appreciably below said temperatures. The second compromise is perhaps the most serious one – during our measurements, it was found that the dominant contributions to the vibrations appear in the general frequency range around 20 kHz. Unfortunately, the accelerometers had a significantly lower calibrated frequency window given by the manufacturers, and therefore had to be used beyond their specifications. This prevented us from making a full quantitative analysis of said vibrations and limited us to relative comparisons only. We note that we do not know of any commercially available accelerometers that would work in cryogenic conditions and cover the entire frequency range needed.

In the end, several practical modifications of the frame supporting the dilution refrigerator and the pulse tube motor plate were found that helped to reduce the vibration levels observed on the mixing chamber plate significantly. This included relatively simple measures, which can be replicated easily in any laboratory, such as decoupling the pulse tube motor plate from the frame of the cryostat and attaching it to the building walls, covering the pipes connecting to the pulse tube compressor with rubber foam, or weighing the cryostat frame down with sandbags. Overall, the publication represents a progress report and it is our hope that more detailed measurements will be performed in the near future, overcoming the limitations imposed by the compromises that had to be made in the present work.

The measurements were performed by DS and AL on the dilution refrigerator installed at the Institut Néel in Grenoble. DS was also responsible for programming the data acquisition software, analysing the data, and for the preparation of the manuscript, with help from EC and AF. Additionally, DS would like to thank P.-E. Roche, who provided the accelerometers.

Appendix A10

D. Schmoranzer, S. Kumar, A. Luck, E. Collin, X. Liu, T. Metcalf, G. Jernigan, A. Fefferman, Observations on Thermal Coupling of Silicon Oscillators in Cryogen-Free Dilution Refrigerators, *J. Low Temp. Phys.* **196**, 268–274 (2019), DOI: 10.1007/s10909-018-02122-1.

This work is part of ongoing investigations into the mechanical properties of amorphous solids at low temperatures, motivated specifically by the proposed universality of the dissipation within amorphous materials due to transitions in atomic two-level systems. The experiments were again performed at the Institut Néel in Grenoble, using sensitive double-paddle oscillators (DPOs) provided by the Naval Research Laboratory group from Washington.

To date, DPOs made of monocrystalline silicon are the most sensitive type of mechanical resonators produced, reaching quality factors of 10^8 at low temperatures in vacuum. Therefore, the DPO is ideally suited to study the mechanics of thin films (of amorphous substances) deposited on its neck – the part undergoing the most severe deformations during the DPO's oscillations. In this study, we have followed the temperature dependence of the frequency shift and dissipation of such DPOs due to thin amorphous silicon films deposited at room temperature.

One of the experimental difficulties with such a measurement is ensuring that the DPO (and the thin film) has the same temperature as is recorded by a thermometer placed on the supporting structure of the DPO or on the mixing chamber plate of a dilution refrigerator. This is usually the case down to several tens of mK, but at lower temperatures, thermal decoupling of the device from its surroundings occurs. This is due to the fact that thermal conductivity of any materials used decreases significantly as temperature drops, while any finite heat leak to the device leads to an ever increasing temperature offset. We have therefore investigated the role of shielding of such an oscillator to minimize the thermal decoupling.

Indeed, we found that an increasing degree of shielding of the device (no shield, a metal screen with holes, and a copper-taped shield permitting no direct line-of-sight) results in a suppression of thermal decoupling, shifting the departure point towards lower temperatures. We have suspected several sources of heating which can lead to this thermal decoupling, including the vibrations of the dry dilution refrigerator (see Appendix A9), as the results obtained on the dry dilution refrigerator were significantly worse than those acquired on a traditional "wet" one. Therefore, a simple test was carried out, whether the thermal decoupling improves when the pulse tube precooling the refrigerator is switched temporarily off. To our surprise, under these conditions, the thermal decoupling of the device became even worse than with the pulse tube running. This situation implies that the decoupling cannot be dominated by vibrations and that other mechanism need to be considered.

The two remaining mechanisms capable of heating up the DPO and causing the decoupling are radiative heat transfer and collisions with residual helium atoms in the vacuum space of the refrigerator. Our results suggest that, contrary to expectation, radiative heat transfer is less important than the direct collisions with helium atoms liberated from the warmer parts of the vacuum space (the top

flange at 300 K, the first stage of the pulse tube at 50 K, or the second stage at 4 K), as the DPO reacts more to the changes in temperature of the above mentioned parts than to the variation of the temperature of the still shield, which might be responsible for radiative heating.

Beyond what is presented in the publication, we have indeed verified this scenario by using a carbon adsorption pump in the vacuum space of the cryostat, which allowed us to directly control the quantity of residual gas atoms. Ultimately, the only solution to really minimize the thermal decoupling of such sensitive devices as the DPOs is to use a dedicated hermetically sealed cell located on the mixing chamber of the dilution refrigerator. This finding may have implications for many low temperature groups worldwide, relying on the ever more popular dry dilution refrigerators to perform their experiments.

The contribution of DS to this work is mainly in the operation of the experimental setup and in data acquisition and analysis, performed jointly with AF, SK, and AL. The publication was prepared by AF and reviewed by EC. The Washington group has provided the DPOs used in this work.

Notes